Prev. Nutr. Food Sci. 2023;28(3):235-245
https://doi.org/10.3746/pnf.2023.28.3.235
ISSN 2287-8602

Unripe *Carica papaya* Fresh Fruit Extract Protects against Methylglyoxal-Mediated Aging in Human Dermal Skin Fibroblasts

Suvara K. Wattanapitayakul[1], Wattanased Jarisarapurin[1,2], Khwandow Kunchana[1], Vasun Setthawong[3,4], and Linda Chularojmontri[5]

[1]Department of Pharmacology, Faculty of Medicine, Srinakharinwirot University, Bangkok 10110, Thailand
[2]National Nanotechnology Center (NANOTEC), National Science and Technology Development Agency (NSTDA), Thailand Science Park, Pathum Thani 12120, Thailand
[3]Department of Surgery, Lerdsin Hospital, Department of Medical Services, Ministry of Public Health, Bangkok 10500, Thailand
[4]Department of Surgery, College of Medicine, Rangsit University, Pathum Thani 12000, Thailand
[5]Department of Preclinical Sciences, Faculty of Medicine, Thammasat University, Pathum Thani 12121, Thailand

ABSTRACT: The glycolytic metabolite methylglyoxal (MGO) initiates the formation of advanced glycation end products and oxidative stress, leading to cellular senescence and skin aging. This study focuses on the anti-aging properties of unripe *Carica papaya* L. (UCP) fresh fruit extract on MGO-induced human dermal fibroblast senescence. We pretreated human foreskin fibroblasts with UCP before incubating them with MGO (400 μM) for 72 h. We used the glycation inhibitor aminoguanidine hydrochloride (AG) as the positive control. Senescent fibroblasts were detected using senescence-associated beta-galactosidase activity and collagen type I expression (COL1A1). We investigated the changes in the Akt, JNK/p38 mitogen-activated protein kinase (MAPK), c-Jun, and nuclear factor kappa B (NF-κB) signaling pathways using Western blotting. UCP significantly suppressed MGO-induced senescent fibroblasts (from 20.90±2.00% to 11.78±2.04%) when compared with the baseline level at 7.10±0.90% ($P<0.05$). While COL1A1 was diminished by 43.35±1.56% ($P<0.001$) in the MGO-treated fibroblasts, UCP and AG could recover COL1A1 to 63.22±4.78% and 64.39±3.34%, respectively. MGO triggered overactivation of Akt, JNK/p38 MAPK, c-Jun, and NF-κB by 2.10±0.09, 8.10±0.37, 6.60±0.29, 2.18±0.23, and 3.74±0.37 folds, respectively. UCP and AG significantly abolished these changes. Consistently, MGO increased matrix metalloproteinase-1 (MMP-1) levels by 2.58±0.04 folds, which was significantly suppressed by UCP and AG pretreatment to 1.87±0.11 and 1.69±0.07 folds, respectively. In summary, UCP controlled MGO-induced fibroblast senescence by suppressing the JNK/c-Jun/MMP and p38/NF-κB/COL1A1 pathways, similar to the action of the glycation inhibitor AG. Therefore, UCP can be considered a functional fruit for preventing and delaying skin aging.

Keywords: carica, collagen, fibroblasts, NF-kappa B, oxidative stress

INTRODUCTION

Excessive sugar consumption and uncontrolled blood glucose levels cause metabolic abnormalities, diabetes, and age-related diseases (Rowan et al., 2018). Hyperglycemia in diabetes is strongly associated with delayed wound healing and increased risk of lower extremity amputation in patients with diabetic foot ulcers (Lane et al., 2020). Hyperglycemia-induced delayed wound healing is caused by oxidative stress, dysregulation of angiogenesis, chronic inflammation, and fibroblast/keratinocyte senescence (Yu et al., 2020; Burgess et al., 2021). The highly reactive dicarbonyl compound methylglyoxal (MGO) is a major glycolytic mediator during hyperglycemia. MGO is a potent glycating agent that reacts non-enzymatically with intracellular biomolecules, such as proteins, lipids, and DNA, forming irreversible advanced glycation end products (AGEs) (Kold-Christensen and Johannsen, 2020), which have been implicated in diabetic complications and impaired wound healing (Shaikh-Kader et al., 2019).

Fibroblasts, the key components of the dermis, reinforce the skin's integrity by producing and maintaining extracellular matrix (ECM) molecules (mainly collagen, proteoglycans, elastin, and cell-binding glycoproteins). Oxidative stress causes cellular senescence and skin aging in fibroblasts, significantly affecting wound repair and the development of chronic wounds (Blair et al., 2020). AGEs-induced reactive oxygen species (ROS) in fibro-

Received 27 March 2023; Revised 2 May 2023; Accepted 22 May 2023; Published online 30 September 2023
Correspondence to Suvara K. Wattanapitayakul, E-mail: suvara@g.swu.ac.th

blasts make the cells enter into a senescent state, characterized by replicative disability and abnormal secretory profile, known as senescence-associated secretory phenotype (SASP). The SASP fibroblasts release several proinflammatory mediators, such as interleukin (IL)-6, IL-8, membrane cofactor proteins, and matrix metalloproteinases (MMPs) that can deteriorate the neighboring cells, degrade the ECM, and promote skin aging (Waldera Lupa et al., 2015). Therefore, anti-aging skin products should focus on preventing or delaying SASP formation (Lim et al., 2017).

Understanding the mechanisms by which MGO induces SASP is essential for studying anti-aging agents. MGO-mediated skin glycation occurs via collagen-targeting AGEs, which send the signal to the receptors of AGEs (RAGEs) (Pageon et al., 2015). Activated RAGEs promote oxidative stress and inflammation by activating PI3K/Akt, JNK/p38 mitogen-activated protein kinase (MAPK), activating protein-1 (AP-1) (c-Jun/c-fos), and nuclear factor kappa B (NF-κB) pathways that can be observed in skin aging and other diabetic complications (Singh et al., 2014). NF-κB is a key transcription factor in SASP that promotes tumor necrosis factor-α (TNF-α) production and MMP expression, which further induces ECM degradation and accelerates skin aging. Additionally, dicarbonyl stress causes c-Jun/AP-1 responsiveness to oxidative stress and downregulates collagen type I (Qin et al., 2014). These synergistic signals activate enhanced senescence-associated beta-galactosidase (SA-β gal), a cellular senescence biomarker. Regardless of the sources of oxidative stress, ROS formation is the hallmark of age-associated skin fibroblast senescence and dysfunction (Lee et al., 2022). Thus, using natural antioxidants as skin protective agents can potentially prevent skin aging by eliminating (senolytics) or neutralizing (senostatics) SASP (Domaszewska-Szostek et al., 2021).

Previous studies showed that unripe *Carica papaya* L. (UCP) fresh fruit extract has a high antioxidant capacity, protecting endothelial cells against oxidative stress (Jarisarapurin et al., 2019). UCP contains well-known antioxidants such as ascorbic and gallic acids and quercetin (Wattanapitayakul et al., 2021). Therefore, we investigated whether UCP could protect against fibroblast oxidative stress induced by MGO, which serves as a model of dicarbonyl stress in diabetic skin deterioration. The inhibitory effects of UCP on fibroblast senescence were compared with that of aminoguanidine hydrochloride (AG), a glycation inhibitor. We also investigated the MGO signaling pathways, such as Akt, JNK/p38 MAPK, c-Jun, NF-κB, and SASP characteristics (MMP-1 production, collagen type I expression, SA-β gal).

MATERIALS AND METHODS

UCP fresh fruit extract preparation

We prepared the fruit juice powder and evaluated certain phyto-antioxidants as previously described (Jarisarapurin et al., 2019). The freeze-dried fruit juice powder was kept at −40°C until use. A stock solution of UCP was freshly prepared for each experiment by dissolving the powder in type 1 sterile ultrapure water (Milli-Q® type 1 ultrapure water systems, MilliporeSigma).

Extraction and identification of human dermal fibroblasts

Foreskin specimens were collected from the Urological Unit, Lerdsin Hospital, Bangkok, Thailand. The research protocols were approved by the Human Research Ethics Committee (No. MOE 0306/13/130). The protocol complied with the Declaration of Helsinki and all tissue donors provided written informed consent. Following the surgical procedure, the foreskin samples from adult donors (aged 20～38) were stored in Dulbecco's Modified Eagle Medium (DMEM), kept on ice, and transported to the laboratory. The extraction was performed as reported previously with minor modifications (Rittié and Fisher, 2005). First, the specimens were washed with 1X Dulbecco's phosphate-buffered saline (DPBS, Thermo Fisher Scientific), cut into small pieces (0.5×0.5 cm^2), and placed in a 60-mm cell culture dish. Small tissue pieces were then incubated within a culture medium containing 2 U/mL of dispase (Thermo Fisher Scientific) and stored at 4°C for 16～21 h. After incubation, the foreskin's epidermis and dermis were separated using sterile forceps. The fibroblasts were extracted from the dermis by flipping the dermal surface down onto a 60-mm cell culture dish containing DMEM supplemented with 10% fetal bovine serum (FBS), 100 U/mL penicillin, and 100 μg/mL streptomycin (Thermo Fisher Scientific), and incubated at 37°C for 5～7 days in a humidified chamber with 5% CO_2. After day 3, a small amount of culture medium was added to the culture dishes to prevent dryness. When the fibroblast outgrowths from tissues were observed, the dermal foreskin tissues were removed, and the cells were washed with 1X DPBS twice. Fibroblasts were further cultured and subcultured till 80% confluency. The cultured cells were maintained for two to three passages before each experiment.

The cultured fibroblasts were identified by morphological characteristics and positive staining with the fibroblast marker vimentin, absent in epithelial or other mesenchymal cells. For the immunohistochemistry, the cells were rinsed with 1X phosphate-buffered saline (PBS) twice and then fixed with 3.7% formaldehyde in PBS for 15 min. After permeabilizing with 0.1% Triton X-100 in PBS for 10 min, the cells were washed thrice with 1X PBS for 10 min on a shaker. The cells were incubated with a

blocking solution [3% bovine serum albumin (BSA) in PBS] for 1 h and then overnight with 1:1,000 Vimentin (#5741, Cell Signaling Technology). After rinsing thrice with 1X PBS, the cells were probed with anti-rabbit IgG (H+L), F(ab')2 Fragment (#4412, Alexa Fluor® 488 Conjugate, Cell Signaling Technology) for 1 h. After incubation and washing, the cells were probed with 10 μM Hoechst 33342 for 30 min (Thermo Fisher Scientific). The fibroblast cells were identified based on their morphology and vimentin-staining using the Olympus FluoView FV10i-confocal laser scanning microscope (Olympus Corp.).

Cell culture and treatment protocols

Human dermal fibroblasts were cultured with DMEM supplemented with 10% FBS, 100 U/mL penicillin, and 100 μg/mL streptomycin in the autoflow NU-4850 humidity control water-jacket laboratory CO_2 incubator (NuAire) maintained under a humidified 5% CO_2 at 37°C. The culture media was replaced every three days until the cells were 80～90% confluent and then were subcultured. For each experiment, the cells were pretreated with various concentrations of UCP (10, 100, 1,000 mg/mL) and 10 mM AG (#396494, Merck KGaA) for 2 h. Then, they were challenged with 400 μM MGO (#M0252, MilliporeSigma) for 0～72 h. After the treatment, the cells were prepared according to each experiment's protocol.

Cell viability

The toxicity of UCP, AG, and MGO was evaluated using the 3-(4,5-dimethylthiazol-2-yl)-2,5-diphenyltetrazolium bromide (MTT) cell viability assay (Bio Basic). We subcultured fibroblasts (1.5×10^4 cells/well) on 96-well cell culture plates for 18～24 h. Then, various concentrations of UCP (0～1,000 μg/mL), AG (0～20 mM), and MGO (0～1,000 μM) dissolved in fresh media were incubated with the cells for 72 h. After that, the cells were incubated with a medium containing MTT (0.25 mg/mL) for 3 h. The cell viability was examined by adding 100% dimethyl sulfoxide (DMSO) to dissolve the formazan crystals generated by the mitochondrial enzymes of the viable fibroblasts. The absorbance was measured at 550 nm using the Synergy H1 Multi-mode reader (Bio Tek). The cell viability percentage was calculated compared to the vehicle-treated group (100%).

Measurement of SA-β gal staining

We used the Senescence Cells Histochemical Staining Kit (MilliporeSigma) to determine whether UCP can prevent MGO-induced fibroblast senescence. Briefly, the cells were grown in 35 mm cell culture plates (2.5×10^5 cells/well) for 18～24 h and then starved by replacing the media containing 1% FBS for 2 h. Then, they were pretreated with various concentrations of UCP (10, 100, 1,000 μg/mL) and AG (10 mM) for 2 h before challenging with 400 μM MGO for 72 h. For the staining, the cells were washed with 1X PBS twice, fixed with 1X fixation buffer, and incubated for 7 min at room temperature. After washing the fixed cells thrice with 1X PBS, the staining mixture was added, and the cells were incubated at 37°C without CO_2 until the blue staining was developed (overnight). The SA-β gal-stained cells were observed under a microscope. Three randomized fields were captured and collected for counting positive and negative stained cells. Data are presented as %SA-β gal compared with the vehicle-treated group (100%).

Measurement of collagen type I alpha 1 chain (COL1A1) expression

We used immunofluorescence staining to evaluate the expression of COL1A1 in the fibroblasts. Briefly, 4×10^4 fibroblasts were cultured on a Nunc™ Lab-Tek™ chamber system (Thermo Fisher Scientific) for 18～24 h. The cells were pretreated with 1,000 μg/mL of UCP and 10 mM of AG for 2 h and challenged with 400 μM MGO for 72 h. Then, the cells were rinsed with 1X PBS twice and fixed with 3.7% formaldehyde in PBS for 15 min. Afterward, they were permeabilized with 0.1% Triton X-100 in PBS for 10 min and washed thrice with 1X PBS for 10 min on a shaker. The cells were blocked using 3% BSA in PBS and incubated for 1 h, followed by probing with 1:1,000 COL1A1 (#39952, Cell Signaling Technology) overnight. The cells were washed thrice with 1X PBS for 10 min and probed with anti-rabbit IgG (H+L), F(ab')2 Fragment (#4412) for 1 h. After washing thrice with 1X PBS, the cells were incubated with 10 μM Hoechst 33342 for 30 min, followed by another three washes. The COL1A1-stained cells were observed under the Olympus FluoView FV10i-confocal laser scanning microscope. We selected five randomized fields to calculate the percent mean fluorescence intensity compared with the vehicle-treated group.

Western blot analysis

The whole cell and nuclear lysates were extracted using RIPA buffer and a Nuclear Extraction Kit (Cat No. 1000 9277, Cayman Chemical), respectively. The protein concentrations were measured using the Bio-Rad protein assay (Bio-Rad Laboratories Ltd.) and equalized to the same amount for each sample. The cell lysate proteins from each sample were separated using SDS-PAGE and then transferred to Amersham Hybond™ P 0.45 PVDF blotting membrane (GE Healthcare) using the Mini-PROTEAN Tetra system (Bio-Rad Laboratories Ltd.). The blotted membranes were soaked in 5% BSA blocking solution in Tris-buffered saline containing 0.1% Tween® 20 detergent (TBST) for 1 h. Then, the blocking buffer was replaced with the primary antibodies 1:1,000 p-Akt (#4051),

Akt (#9272), p-p38 (#9215), p38 (#8690), p-JNK (#4668), JNK (#9252), NF-κB (#4764), phospho-c-Jun (p-c-Jun) (#9164), MMP-1 (#54376), or β-actin (#3700) (Cell Signaling Technology) and incubated overnight. After washing the membranes thrice (10 min each) with 1×TBST, they were incubated with 1:3,000 anti-rabbit (#7076) or anti-mouse (#7074) IgG linked with HRP (Cell Signaling Technology) for 1 h. After soaking in 1×TBST, the specific protein bands on the membranes were probed with Amersham ECL Select Western Blot Reagent (GE Healthcare) and detected by a Gel Documentation System (UVITEC). The bands were quantified and analyzed using ImageJ version 1.53k (National Institutes of Health, https://imagej.net/ImageJ1).

Statistical analysis

The statistical difference between the means of independent groups and between sample groups was analyzed using one-way ANOVA and *t*-test, respectively. The *P*-values of <0.05 was set for statistical significance. Data are presented as mean±SEM calculated from at least three experiments.

RESULTS

Identification of fibroblasts extracted from human foreskin

Cell morphology analysis showed elongated spindle-shaped cells with processes extending from the cell body. Immunofluorescence results showed these cells were also positive for the biomarker vimentin, a filament protein expressed in fibroblasts (Fig. 1).

Effects of UCP, AG, and MGO on cell viability

Treatment with UCP (100~1,000 μg/mL) and AG (1~20 mM) did not have any toxic effects on fibroblasts after 72 h incubation (Fig. 2A and 2B). However, treatment with 600, 700, 800, and 1,000 μg/mL of MGO significantly decreased the cell viability to 91.27±0.07%, 90.74±1.42%, 88.46±0.04%, 43.26±2.81%, and 5.89±0.32%, respectively compared with the vehicle-treated group (Fig. 2C).

Effect of UCP on MGO-induced fibroblast senescence

The blue stained SA-β gal-positive cells, used as senescence markers, could be visualized under a light microscope (Fig. 3A). The basal levels of senescent cells (vehicle-treated groups) were 7.1±0.9%, while 400 μM MGO significantly increased SA-β gal-positive fibroblasts to 20.9±2% (P<0.001). UCP treatment alone had a negligible impact on fibroblast senescence. However, fibroblasts pre-incubated with UCP (1,000 μg/mL) before MGO insult showed significantly lower senescence (11.78±2.04%) than the vehicle control, or 43.6% lower than the MGO-treated group (P<0.05). While lower UCP concentrations (10 and 100 μg/mL) dose-dependently reduced SA-β gal-positive cells (19.6±2.34% and 18.3±2.97%, respectively), the results were not statistically significant. When 10 mM of AG, a glycation inhibitor, was added to the fibroblasts, it significantly attenuated MGO-induced fibroblast cell senescence to 11.6±2.53% (Fig. 3B).

Effect of UCP on COL1A1 expression in MGO-induced fibroblast cell senescence

We used immunofluorescent staining to evaluate the effect of MGO on the COL1A1 protein expression in the fibroblasts. Fig. 4A represents fibroblasts stained with Hoechst (blue) and COL1A1 (green) in each treatment group. While the UCP and AG-treated fibroblasts were unaffected, MGO significantly decreased the relative fluorescence intensity percentage to 43.35±1.56% compared

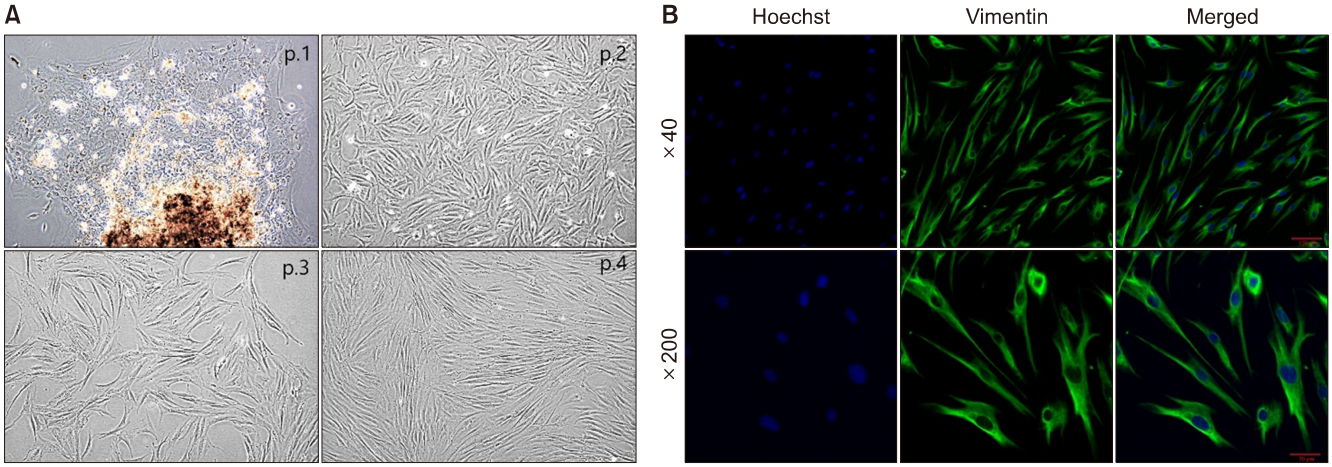

Fig. 1. Isolation and identification of primary culture of human dermal fibroblasts. (A) Representative photographs of fibroblasts extracted from human foreskin at different passages (p.) (magnification, ×100). (B) Confocal microscopy images of Hoechst and vimentin immunofluorescent staining (magnification, ×40 and ×200).

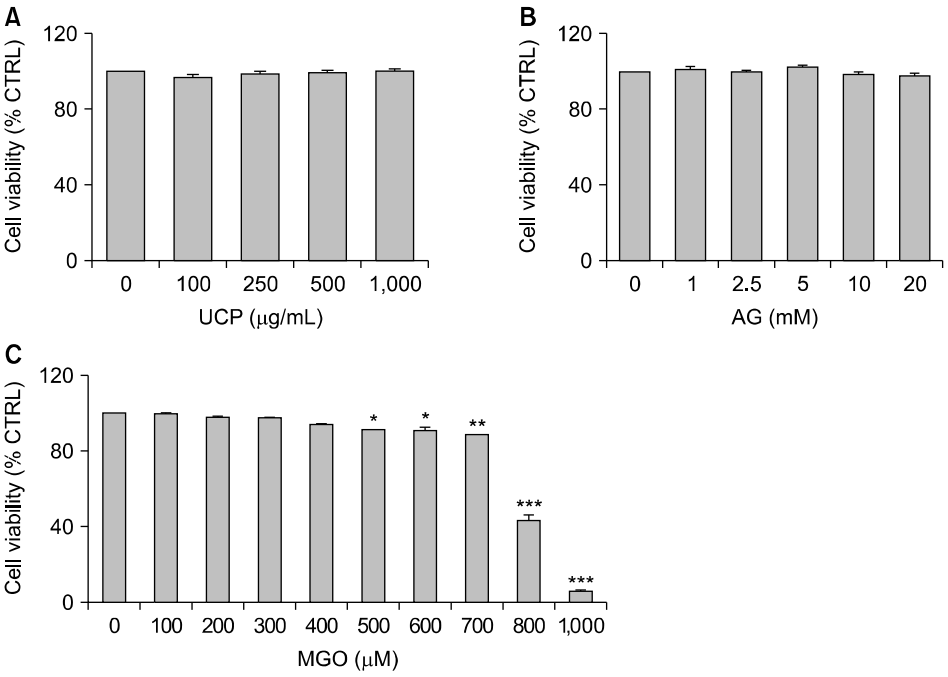

Fig. 2. Effects of unripe *Carica papaya* L. (UCP), aminoguanidine hydrochloride (AG), and methylglyoxal (MGO) on cell viability of fibroblasts. Fibroblasts were incubated with various concentrations of (A) UCP, (B) AG, and (C) MGO for 72 h. Data are presented as mean±SEM of n≥3. $^{*}P<0.05$, $^{**}P<0.01$, and $^{***}P<0.001$ compared with the vehicle-treated group (control, CTRL=100%).

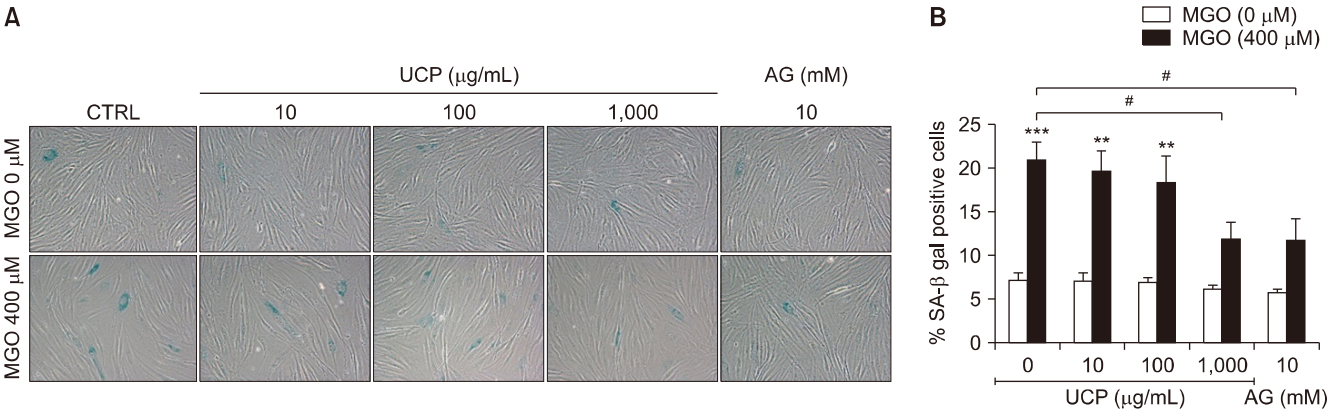

Fig. 3. Effect of unripe *Carica papaya* L. (UCP) and aminoguanidine hydrochloride (AG) on methylglyoxal (MGO)-induced senescent fibroblast. (A) The representative photographs of senescence-associated beta-galactosidase (SA-β gal)-stained fibroblasts with visualized under a light microscope. The SA-β gal-positive cells are shown in blue. (B) A graphical representation of the %SA-β gal-positive cells in each treatment group. Data are presented as mean±SEM of n≥3. $^{**}P<0.01$ and $^{***}P<0.001$ compared with the vehicle-treated group. $^{\#}P<0.05$ compared with the MGO-treated group. CTRL, control.

with the vehicle-treated group (100%) ($P<0.001$). Pretreatment with UCP (1,000 mg/mL) and AG (10 mM) significantly increased the % intensity of COL1A1 to 63.22±4.78% and 64.39±3.34% at $P<0.05$ and $P<0.01$, respectively, when compared with MGO-treated group (Fig. 4B).

Time-course study of Akt, p38, JNK, NF-κB signaling, and MMP-1 protein levels in fibroblasts treated with MGO

Based on the band intensity on the Western blot (Fig. 5A), we calculated the fold changes in several proteins in fibroblasts incubated with MGO 400 μM from 0 to 72 h (Fig. 5B~5G). For the cytosolic signal transduction proteins, MGO activated the phosphorylation of Akt, p38, and JNK as early as 0.5 h, which subsided later. The relative p-Akt/Akt ratios rose significantly to 2.30±0.18 and 1.76±0.07 folds after the MGO challenge at 0.5 and 1 h, respectively. The activation of MAPK signaling through p38 and JNK peaked at 0.5 h with relative phosphorylation changes to 5.29±0.43 and 3.96±0.60 folds ($P<0.05$), respectively (Fig. 5B and 5C). Similarly, phosphorylation of c-Jun, which acts downstream from JNK, was significantly increased for a longer timeframe to 3.41±0.43, 4.20±0.28, and 2.87±0.10 folds ($P<0.05$) at 0.5, 1, and 2 h, respectively (Fig. 5D). MGO also stimulated and maintained the inflammatory mediator NF-κB translocation into the nucleus for 24 h. Statistically significant fold changes were observed in the activation after MGO incubation at 0.5, 1, 2, 4, 12, and 24 h at 1.69±0.07, 2.39±0.13, 2.07±0.07, 2.16±0.16, 2.03±0.17, and 2.43±0.20 ($P<0.05$), respectively (Fig. 5F). The maximum increase in the stress-activated protein MMP-1 was at 72 h

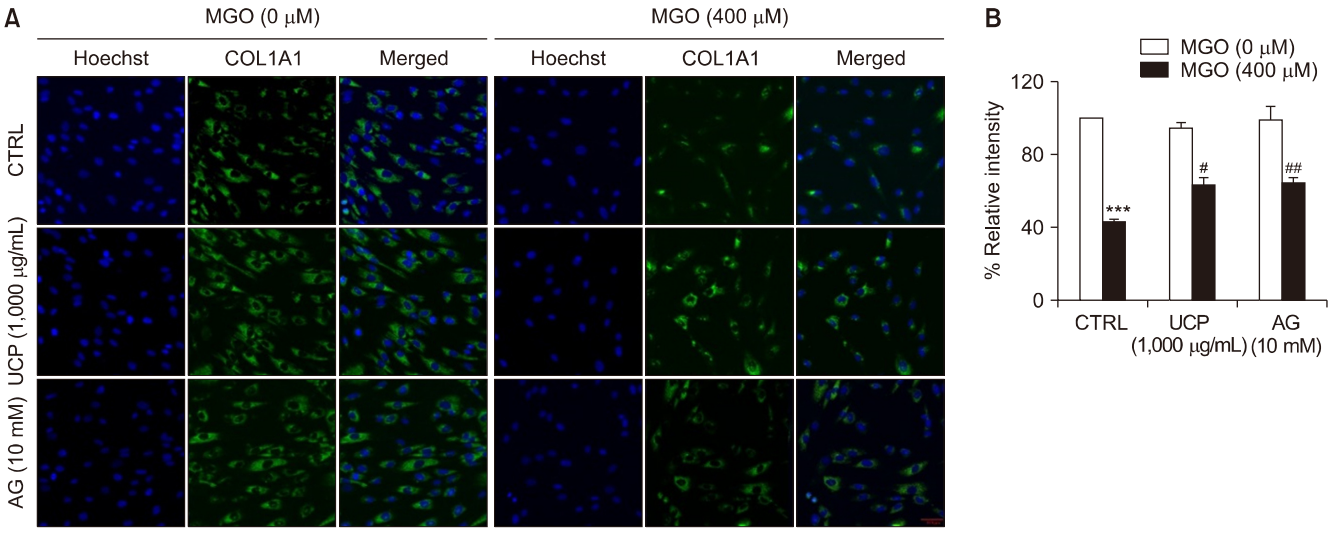

Fig. 4. Effect of unripe *Carica papaya* L. (UCP) and aminoguanidine hydrochloride (AG) pretreatment on collagen type I alpha 1 chain (COL1A1) expression in methylglyoxal (MGO)-induced senescent fibroblasts. (A) Confocal microscopy images of Hoechst and COL1A1 stained fibroblasts. (B) Graphical representation of relative fluorescence intensity (COL1A1 levels) of each treatment group. Data are presented as mean±SEM of n≥3. ***P<0.001 compared to the vehicle-treated group (control, CTRL). $^{\#}P$<0.05 and $^{\#\#}P$<0.01 compared with the MGO-treated group.

to 3.51±0.57 folds (Fig. 5G). Therefore, this time point was chosen to subsequently investigate the effects of UCP on each signaling protein in MGO-induced fibroblast senescence during the time-course study.

Effect of UCP pretreatment on p-Akt and MAPK pathways in MGO-induced cell senescence

The Western blot bands of p-Akt/Akt, p-p38/p38, and p-JNK/JNK ratios are shown in Fig. 6A and represented significantly higher ratios in the fibroblasts challenged with 400 μM MGO, at 2.1±0.09, 8.1±0.37, and 6.6±0.29 (P<0.01), respectively (Fig. 6) than the vehicle-treated group (1.00±0.22). Pretreatment with UCP and AG reversed the effects of MGO by significantly decreasing p-Akt/Akt to 1.59±0.11 and 1.32±0.16 (P<0.05; Fig. 6B). Similarly, the p-p38/p38 ratios were significantly decreased to 5.56±0.44 and 2.90±0.28, respectively (Fig. 6C). Further, p-JNK signaling was significantly attenuated to 4.79±0.29 and 1.94±0.48, respectively, compared with the MGO-treated group (Fig. 6D).

Effect of UCP pretreatment on NF-κB and p-c-Jun pathways in MGO-induced fibroblast cell senescence

Fig. 7A shows the Western blot band results. NF-κB and p-c-Jun were significantly activated in the fibroblasts exposed to 400 μM MGO by 2.18±0.23 and 3.74±0.37 folds (P<0.001), respectively, compared with the vehicle-treated group. UCP pretreatment significantly suppressed NF-κB/β-actin and p-c-Jun/β-actin ratio to 0.98±0.17 and 2.48±0.37, respectively, compared with the MGO-treated group. Similarly, the NF-κB/β-actin and p-c-Jun/β-actin ratios were significantly lower (1.35±0.12 and 1.43±0.21, respectively, P<0.01) in the AG pretreated cells than the MGO-treated group (Fig. 7B and 7C).

Effects of UCP and AG pretreatment on MMP-1 in MGO-induced fibroblast senescence

Fig. 8 shows the changes in MMP-1 protein expression after MGO-induced fibroblast stress. MGO significantly elevated the MMP-1 levels by 2.58±0.04 folds (P<0.001) compared with the vehicle-treated group. MMP-1/β-actin ratio was significantly reduced in the UCP and AG pretreated cells, down to 1.87±0.11 and 1.69±0.07 (P<0.01 and P<0.001, respectively) than the MGO-treated group.

DISCUSSION

Loss of glycemic control, which mainly contributes to diabetes complications, is characterized by oxidative stress, inflammation, cell instability, and cellular senescence. MGO is a highly reactive glucose metabolite that induces the formation of AGEs and contributes to the pathology of diabetes and the pathogenesis of AGEs-related diseases (Rowan et al., 2018). Excessive MGO causes structural protein damage and delayed wound healing via the mechanisms involving structural changes and fibroblast dysfunction attributed to cell senescence. This study demonstrates that the functional fruit extract from UCP inhibited MGO-activated senescence phenotype, suppressed MMP-1 expression, and reduced collagen degradation. UCP attenuated MGO-induced JNK/p38 MAPK pathway activation, NF-κB, and AP-1 in human dermal fibroblasts. Therefore, this model of MGO-activated dicarbonyl stress in fibroblasts showing cellular senescence

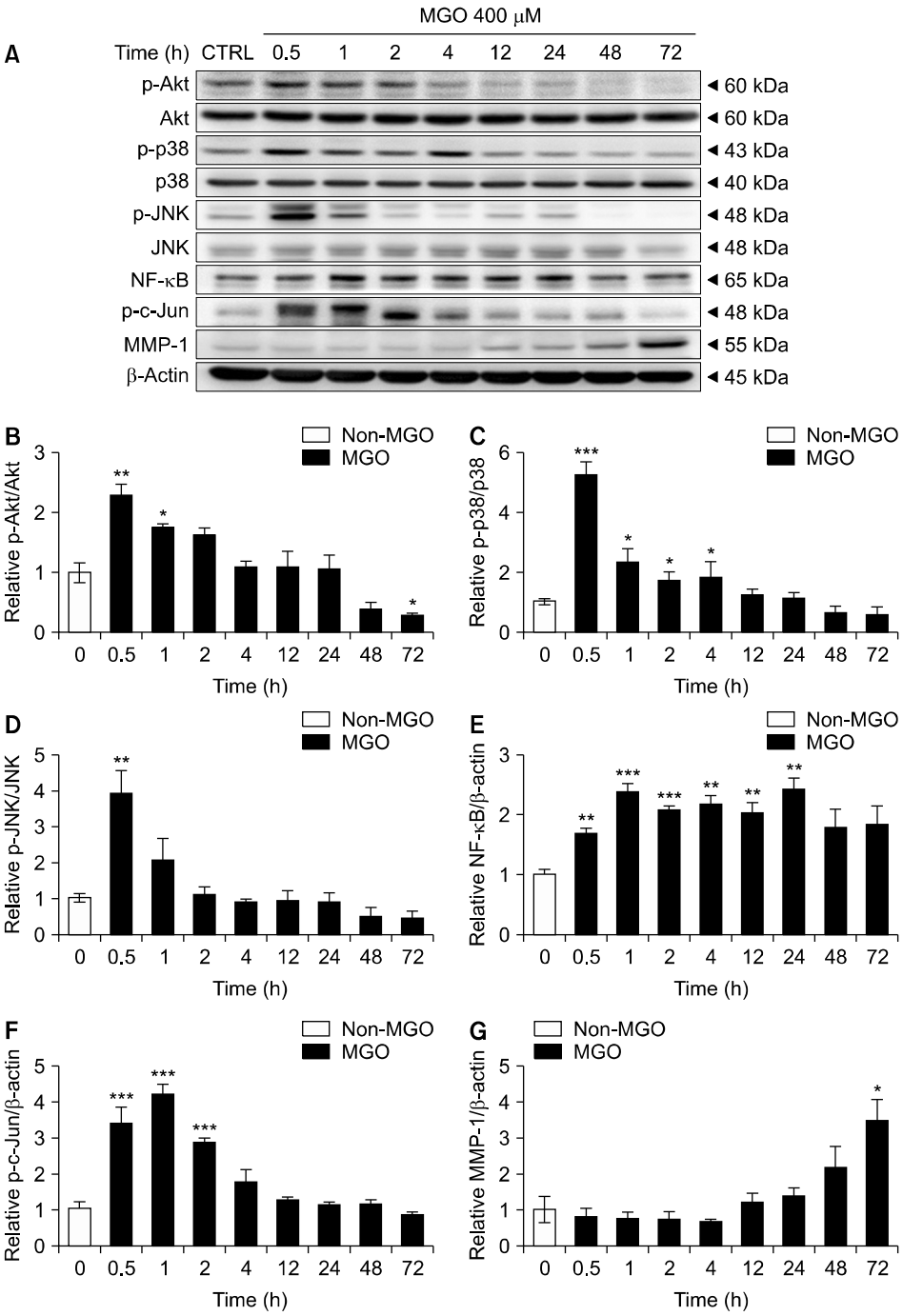

Fig. 5. Time-course study of the effect of methylglyoxal (MGO) on cell signaling and matrix metalloproteinases-1 (MMP-1) protein levels in fibroblasts. (A) Representative Western blot bands for each antibody probe as indicated in the labels. Relative ratios of (B) p-Akt/Akt, (C) p-p38/p38, (D) p-JNK/JNK, (E) nuclear factor kappa B (NF-κB)/β-actin, (F) phospho-c-Jun (p-c-Jun)/β-actin, and (G) MMP-1/β-actin. Data are presented as mean±SEM of n≥3. *P<0.05, **P<0.01, and ***P<0.001 compared with the vehicle-treated group. CTRL, control.

and impaired function is appropriate and can be widely used for investigating the potential substances that can modify AGEs-related complications.

Herein, we used human dermal fibroblast cells isolated from adult foreskins for *in vitro* studies using vimentin, a common molecular marker for fibroblasts, to identify fibroblasts reliably (Chang et al., 2014). We identified the non-toxic doses of AG (1～20 mM) and UCP (100～1,000 μg/mL). We observed that fibroblast senescence was induced within 72 h after incubation with 400 μM MGO, mimicking previously reported conditions (Sejersen and Rattan, 2009). The appearance of senescence-associated marker (SA-β-gal) was confirmed in aged cells and has been commonly used to determine the cellular senescence of fibroblasts (Zorina et al., 2022). Dicarbonyl stress triggers age-mediated signaling cascades via the production of AGEs, and excessive intracellular ROS correlated with age-related and chronic diseases (Ott et al., 2014). Prolonged incubation of fibroblasts with MGO elicited a senescence phenotype similar to that after accumulation of dicarbonyl stress, as indicated by the positive SA-β gal-stained cells. Further, the down-regulation of the major ECM protein collagen type I (encoded by COL1A1 and COL1A2) might be due to fibroblast dysfunction, which is implicated in skin aging and wound healing (Yang et al., 2020). Pretreatment with UCP and the AGE inhibi-

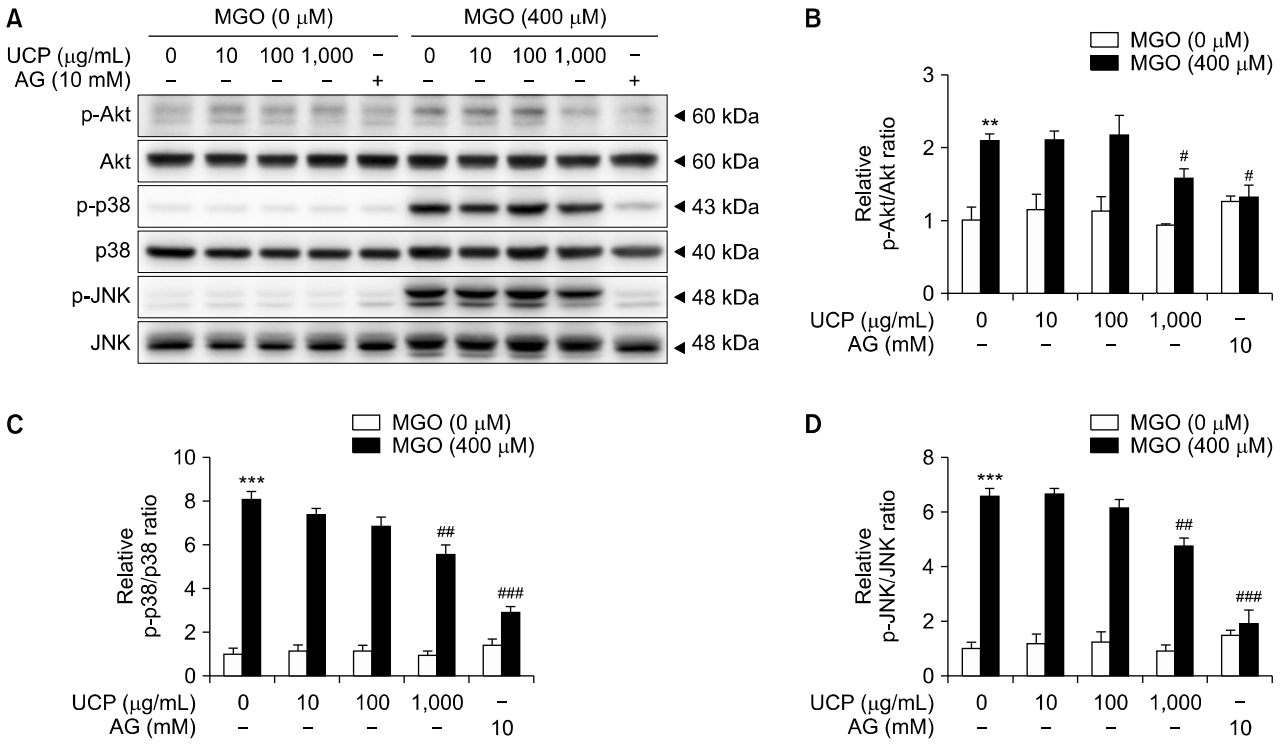

Fig. 6. Effect of unripe *Carica papaya* L. (UCP) and aminoguanidine hydrochloride (AG) pretreatment on Akt and mitogen-activated protein kinase (MAPK) signaling pathways in methylglyoxal (MGO)-induced senescent fibroblasts. (A) Representative Western blot protein bands of each treatment group. Relative ratios of (B) p-Akt/Akt, (C) p-p38/p38, and (D) p-JNK/JNK. Data are presented as mean±SEM of n≥3. $^{**}P<0.01$ and $^{***}P<0.001$ compared with the vehicle-treated group. $^{\#}P<0.05$, $^{\#\#}P<0.01$, and $^{\#\#\#}P<0.001$ compared with the MGO-treated group.

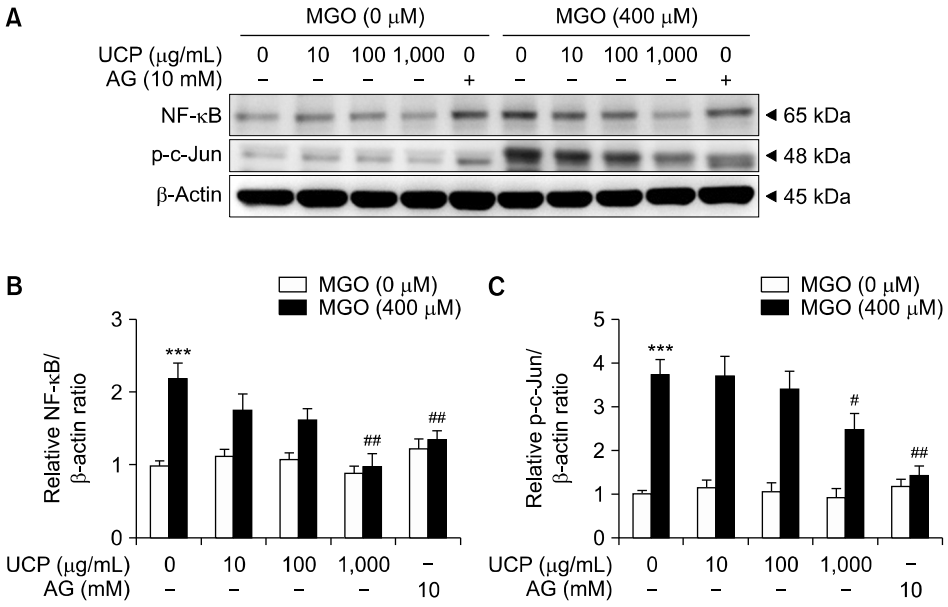

Fig. 7. Effect of unripe *Carica papaya* L. (UCP) pretreatment on nuclear factor kappa B (NF-κB) and phospho-c-Jun (p-c-Jun) signaling proteins in methylglyoxal (MGO)-induced senescent fibroblasts. (A) Representative Western blot bands for each treatment group. (B) Relative ratios of NF-κB/β-actin and (C) p-c-Jun/β-actin. Data are presented as mean±SEM of n≥3. $^{***}P<0.001$ compared to the vehicle-treated group. $^{\#}P<0.05$ and $^{\#\#}P<0.01$ compared with the MGO-treated group.

tor AG decreased the senescence-positive cells and collagen production, as indicated by a reduction in the molecular markers, suggesting their anti-aging potential. AG can rapidly react with dicarbonyl compounds to protect against AGE formation (Thornalley, 2003). Thus, AG prevents AGE accumulation and disrupts the downstream signaling cascades causing cell senescence (Sato et al., 2022). The anti-aging effect of UCP on MGO-induced cell senescence is similar to that of AG. Several natural compounds reduce the formation of AGEs mainly by trapping the active dicarbonyl compounds, regulating RAGE, or scavenging ROS (Song et al., 2021). UCP exerts high antioxidant potential by scavenging excessive ROS, thus protecting against MGO-induced fibroblast oxidative stress (Wattanapitayakul et al., 2021).

MGO mediates AGE formation with the cooperation of ROS, which further triggers PI3K/Akt and JNK/p38 MAPK and their downstream signaling cascades. Al-

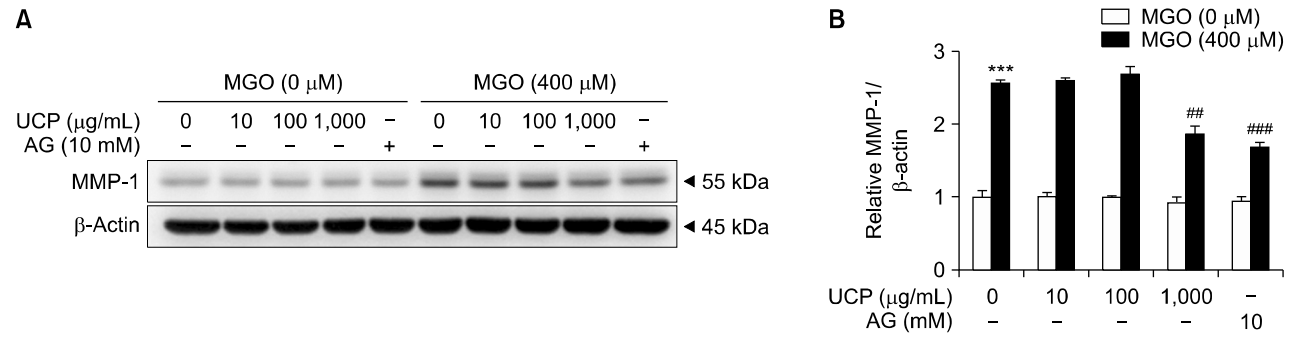

Fig. 8. Effects of unripe *Carica papaya* L. (UCP) and aminoguanidine hydrochloride (AG) on matrix metalloproteinases-1 (MMP-1)/β-actin ratio in methylglyoxal (MGO)-induced fibroblast senescence. (A) Representative Western blot bands for each treatment group. (B) Relative MMP-1/β-actin ratios. Data are presented as mean±SEM of n≥3. $^{***}P<0.001$ compared to the vehicle-treated group. $^{\#\#}P<0.01$ and $^{\#\#\#}P<0.001$ compared with the MGO-treated group.

though we could not quantify the ROS produced in the fibroblasts, our results suggested that MGO-induced oxidative stress by enhancing the downstream ROS signaling cascade, as indicated by the presence of biomarkers of skin aging SA-β-Gal and SASP (represented by MMPs) (Papaconstantinou, 2019; Gu et al., 2020). Akt is a ubiquitous signal transducer that regulates growth, proliferation, cell survival, and senescence. At optimal levels, Akt determines the cell fate and direction toward survival or adaptation. In fibroblasts, Akt plays a central role in senescence phenotype by enhancing ROS formation via NOX4, activating NF-κB, and mediating p53-induced secretion of SASP factors, such as IL-6 and IL-8 (Kim et al., 2017). Under high MGO conditions, Akt is over-phosphorylated, which activates stress-associated JNK/p38 MAPK, disrupting the survival signal and shifting the cells toward the senescence phenotype. Like Akt, the stress response MAPK is stimulated at a very early stage after MGO exposure. The downstream signaling networks involved in the phenotypic changes of senescent cells are often associated with AP-1 and NF-κB, which subsequently trigger SASP. NF-κB activation, observed in senescent fibroblasts, triggers TNF-α secretion and JNK activation (Yosef et al., 2017). JNK transduces the signal to AP-1 and mediates MMP-3, IL-6, and IL-8 expression (Song et al., 2019). p38 MAPK induces premature senescence phenotype in skin fibroblasts and downregulates COL1A1 (Jeon et al., 2021). Like other natural substances from *Dendrobium nobile* Lindl., UCP withheld MGO-induced fibroblast senescence by suppressing the JNK/c-Jun/MMPs and p38/NF-κB/COL1A1 axes (Bigot et al., 2012; Terazawa et al., 2021; Li et al., 2022).

The release and production of MMPs, which are SASP factors, are increased in senescent cells, causing the degradation of structural proteins. Similar to SA-β gal, SASP is also used as a senescent biomarker for investigating cell senescence (Wang and Dreesen, 2018). Increased production of the collagenase MMP-1 in aged fibroblasts increases the degradation of collagen type I, a key structural component of the skin, steering toward skin aging (Henriksen and Karsdal, 2016). Here, we observed increased MMP-1 expression in MGO-exposed fibroblasts, while UCP pretreatment abolished MMP-1 activation. Moreover, MGO activated NF-κB and AP-1, suppressing intracellular COL1A1 synthesis, while UCP could prevent this collagen loss. Similar to a previous study, the application of a natural product, urolithin A, to replicative senescent fibroblasts increased COL1A1 expression and reduced MMP-1 expression (Liu et al., 2019). Therefore, the therapeutic strategies for senescence-associated diseases could target the SASP factors by blocking the induction of the signaling cascade and release of secretory factors (Watanabe et al., 2017). Antioxidant and anti-inflammatory effects correlate significantly with skin anti-aging because ROS is a major driver of aging. Thus, compounds with antioxidative effects can be considered as potentially anti-aging agents. UCP exhibits its potent antioxidant and anti-inflammatory effect by inhibiting NF-κB signaling and its anti-senescence activity by preventing MGO-induced human dermal fibroblast aging through decreasing AGEs-associated cell signaling pathways.

In summary, UCP exerts its anti-aging effect by decreasing the AGEs-mediated cell signaling pathways. UCP ablated Akt, p38/JNK, AP-1, and NF-κB signaling pathways associated with fibroblast senescence (Fig. 9). MGO-challenged fibroblasts pretreated with UCP exhibit decreased production of SASP factor and MMP-1, but increased collagen synthesis. We showed that UCP can prevent age-related diseases, such as skin aging, due to its abundant antioxidants. Therefore, consuming nutraceuticals containing various bioactive compounds with antioxidant, anti-inflammatory, and anti-aging properties can delay age-related disease and prolong human life (Dhalaria et al., 2020). Further studies should be conducted to validate using UCP as a supplement or a nutraceutical and a functional fruit for anti-aging.

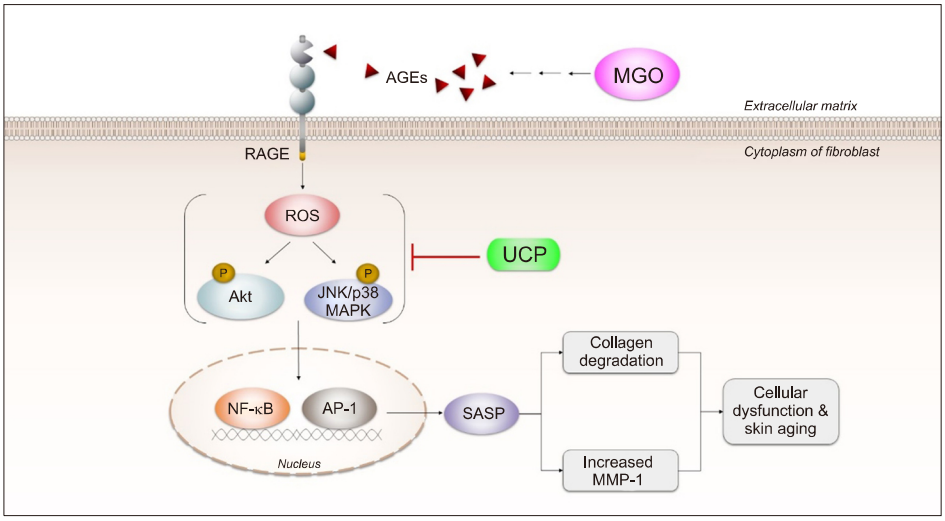

Fig. 9. Graphical representation of the proposed mechanism of unripe *Carica papaya* L. (UCP) preventing skin fibroblast senescence. First, methylglyoxal (MGO) activates advanced glycation end product (AGE) formation, leading to AGEs-receptors of AGEs (RAGEs) binding and reactive oxygen species (ROS) generation. Then, ROS triggers oxidative stress signaling cascades, including Akt and JNK/p38 mitogen-activated protein kinase (MAPK), which further stimulate NF-κB and activating protein-1 (AP-1)-mediated transcription of senescence-associated genes. Resultantly, fibroblasts exhibit senescence-associated secretory phenotype (SASP) characteristics, such as production of matrix metalloproteinases-1 (MMP-1) and other collagen-degrading enzymes. Finally, fibroblasts enter the cellular senescence, triggering their dysfunction and aging. UCP antagonizes MGO-induced fibroblast senescence through its ROS scavenging property and by inhibiting the upstream Akt, JNK/p38 MAPK signaling cascade, which suppresses SASP and fibroblast senescence.

FUNDING

This research was funded by research grants from Faculty of Medicine, Srinakharinwirot University (grant numbers: 406/2564 and 139/2565).

AUTHOR DISCLOSURE STATEMENT

The authors declare no conflict of interest.

AUTHOR CONTRIBUTIONS

Concept and design: SKW, WJ. Analysis and interpretation: WJ, SKW, LC. Data collection: WJ, KK, VS. Writing the article: WJ, SKW. Critical revision of the article: all authors. Final approval of the article: all authors. Statistical analysis: WJ. Obtained funding: SKW. Overall responsibility: SKW.

REFERENCES

Bigot N, Beauchef G, Hervieu M, Oddos T, Demoor M, Boumediene K, et al. NF-κB accumulation associated with *COL1A1 trans*-activators defects during chronological aging represses type I collagen expression through a -112/-61-bp region of the *COL1A1* promoter in human skin fibroblasts. J Invest Dermatol. 2012. 132:2360-2367.

Blair MJ, Jones JD, Woessner AE, Quinn KP. Skin structure-function relationships and the wound healing response to intrinsic aging. Adv Wound Care. 2020. 9:127-143.

Burgess JL, Wyant WA, Abdo Abujamra B, Kirsner RS, Jozic I. Diabetic wound-healing science. Medicina. 2021. 57:1072. https://doi.org/10.3390/medicina57101072

Chang Y, Li H, Guo Z. Mesenchymal stem cell-like properties in fibroblasts. Cell Physiol Biochem. 2014. 34:703-714.

Dhalaria R, Verma R, Kumar D, Puri S, Tapwal A, Kumar V, et al. Bioactive compounds of edible fruits with their anti-aging properties: a comprehensive review to prolong human life. Antioxidants. 2020. 9:1123. https://doi.org/10.3390/antiox9111123

Domaszewska-Szostek A, Puzianowska-Kuźnicka M, Kuryłowicz A. Flavonoids in skin senescence prevention and treatment. Int J Mol Sci. 2021. 22:6814. https://doi.org/10.3390/ijms22136814

Gu Y, Han J, Jiang C, Zhang Y. Biomarkers, oxidative stress and autophagy in skin aging. Ageing Res Rev. 2020. 59:101036. https://doi.org/10.1016/j.arr.2020.101036

Henriksen K, Karsdal MA. Type I collagen. In: Karsdal MA, editor. Biochemistry of Collagens, Laminins and Elastin: Structure, Function and Biomarkers. Academic Press. 2016. p 1-11.

Jarisarapurin W, Sanrattana W, Chularojmontri L, Kunchana K, Wattanapitayakul SK. Antioxidant properties of unripe *Carica papaya* fruit extract and its protective effects against endothelial oxidative stress. Evid Based Complement Alternat Med. 2019. 2019:4912631. https://doi.org/10.1155/2019/4912631

Jeon S, Yoon YS, Kim HK, Han J, Lee KM, Seol JE, et al. Ablation of CRBN induces loss of type I collagen and SCH in mouse skin by fibroblast senescence via the p38 MAPK pathway. Aging. 2021. 13:6406-6419.

Kim YY, Jee HJ, Um JH, Kim YM, Bae SS, Yun J. Cooperation between p21 and Akt is required for p53-dependent cellular senescence. Aging Cell. 2017. 16:1094-1103.

Kold-Christensen R, Johannsen M. Methylglyoxal metabolism and aging-related disease: moving from correlation toward causation. Trends Endocrinol Metab. 2020. 31:81-92.

Lane KL, Abusamaan MS, Voss BF, Thurber EG, Al-Hajri N, Gopakumar S, et al. Glycemic control and diabetic foot ulcer

outcomes: A systematic review and meta-analysis of observational studies. J Diabetes Complications. 2020. 34:107638. https://doi.org/10.1016/j.jdiacomp.2020.107638

Lee JH, Park J, Shin DW. The molecular mechanism of polyphenols with anti-aging activity in aged human dermal fibroblasts. Molecules. 2022. 27:4351. https://doi.org/10.3390/molecules27144351

Li W, Mu X, Wu X, He W, Liu Y, Liu Y, et al. *Dendrobium nobile* Lindl. polysaccharides protect fibroblasts against UVA-induced photoaging via JNK/c-Jun/MMPs pathway. J Ethnopharmacol. 2022. 298:115590. https://doi.org/10.1016/j.jep.2022.115590

Lim H, Park BK, Shin SY, Kwon YS, Kim HP. Methyl caffeate and some plant constituents inhibit age-related inflammation: effects on senescence-associated secretory phenotype (SASP) formation. Arch Pharm Res. 2017. 40:524-535.

Liu CF, Li XL, Zhang ZL, Qiu L, Ding SX, Xue JX, et al. Antiaging effects of urolithin A on replicative senescent human skin fibroblasts. Rejuvenation Res. 2019. 22:191-200.

Ott C, Jacobs K, Haucke E, Navarrete Santos A, Grune T, Simm A. Role of advanced glycation end products in cellular signaling. Redox Biol. 2014. 2:411-429.

Pageon H, Zucchi H, Dai Z, Sell DR, Strauch CM, Monnier VM, et al. Biological effects induced by specific advanced glycation end products in the reconstructed skin model of aging. Biores Open Access. 2015. 4:54-64.

Papaconstantinou J. The role of signaling pathways of inflammation and oxidative stress in development of senescence and aging phenotypes in cardiovascular disease. Cells. 2019. 8:1383. https://doi.org/10.3390/cells8111383

Qin Z, Robichaud P, He T, Fisher GJ, Voorhees JJ, Quan T. Oxidant exposure induces cysteine-rich protein 61 (CCN1) via c-Jun/AP-1 to reduce collagen expression in human dermal fibroblasts. PLoS One. 2014. 9:e115402. https://doi.org/10.1371/journal.pone.0115402

Rittié L, Fisher GJ. Isolation and culture of skin fibroblasts. Methods Mol Med. 2005. 117:83-98.

Rowan S, Bejarano E, Taylor A. Mechanistic targeting of advanced glycation end-products in age-related diseases. Biochim Biophys Acta Mol Basis Dis. 2018. 1864:3631-3643.

Sato F, Wong CP, Furuya K, Kuzu C, Kimura R, Udo T, et al. Anti-skin aging activities of *Sideritis scardica* and 3 flavonoids with an uncommon 8-hydroxyl moiety. Nat Prod Commun. 2022;17:1-10. https://doi.org/10.1177/1934578X221094910

Sejersen H, Rattan SI. Dicarbonyl-induced accelerated aging in vitro in human skin fibroblasts. Biogerontology. 2009. 10:203-211.

Shaikh-Kader A, Houreld NN, Rajendran NK, Abrahamse H. The link between advanced glycation end products and apoptosis in delayed wound healing. Cell Biochem Funct. 2019. 37:432-442.

Singh VP, Bali A, Singh N, Jaggi AS. Advanced glycation end products and diabetic complications. Korean J Physiol Pharmacol. 2014. 18:1-14.

Song HK, Noh EM, Kim JM, You YO, Kwon KB, Lee YR. Reversine inhibits MMP-3, IL-6 and IL-8 expression through suppression of ROS and JNK/AP-1 activation in interleukin-1β-stimulated human gingival fibroblasts. Arch Oral Biol. 2019. 108:104530. https://doi.org/10.1016/j.archoralbio.2019.104530

Song Q, Liu J, Dong L, Wang X, Zhang X. Novel advances in inhibiting advanced glycation end product formation using natural compounds. Biomed Pharmacother. 2021. 140:111750. https://doi.org/10.1016/j.biopha.2021.111750

Terazawa S, Takada M, Sato Y, Nakajima H, Imokawa G. The attenuated secretion of hyaluronan by UVA-exposed human fibroblasts is associated with up- and downregulation of HYBID and HAS2 expression via activated and inactivated signaling of the p38/ATF2 and JAK2/STAT3 cascades. Int J Mol Sci. 2021. 22:2057. https://doi.org/10.3390/ijms22042057

Thornalley PJ. Use of aminoguanidine (Pimagedine) to prevent the formation of advanced glycation endproducts. Arch Biochem Biophys. 2003. 419:31-40.

Waldera Lupa DM, Kalfalah F, Safferling K, Boukamp P, Poschmann G, Volpi E, et al. Characterization of skin aging-associated secreted proteins (SAASP) produced by dermal fibroblasts isolated from intrinsically aged human skin. J Invest Dermatol. 2015. 135:1954-1968.

Wang AS, Dreesen O. Biomarkers of cellular senescence and skin aging. Front Genet. 2018. 9:247. https://doi.org/10.3389/fgene.2018.00247

Watanabe S, Kawamoto S, Ohtani N, Hara E. Impact of senescence-associated secretory phenotype and its potential as a therapeutic target for senescence-associated diseases. Cancer Sci. 2017. 108:563-569.

Wattanapitayakul SK, Kunchana K, Jarisarapurin W, Chularojmontri L. Screening of potential tropical fruits in protecting endothelial dysfunction *in vitro*. Food Nutr Res. 2021. 65. https://doi.org/10.29219/fnr.v65.7807

Yang Y, Li Z, Guo J, Xu Y. Deacetylation of MRTF-A by SIRT1 defies senescence induced down-regulation of collagen type I in fibroblast cells. Biochim Biophys Acta Mol Basis Dis. 2020. 1866:165723. https://doi.org/10.1016/j.bbadis.2020.165723

Yosef R, Pilpel N, Papismadov N, Gal H, Ovadya Y, Vadai E, et al. p21 maintains senescent cell viability under persistent DNA damage response by restraining JNK and caspase signaling. EMBO J. 2017. 36:2280-2295.

Yu J, Nam D, Park KS. Substance P enhances cellular migration and inhibits senescence in human dermal fibroblasts under hyperglycemic conditions. Biochem Biophys Res Commun. 2020. 522:917-923.

Zorina A, Zorin V, Kudlay D, Kopnin P. Age-related changes in the fibroblastic differon of the dermis: role in skin aging. Int J Mol Sci. 2022. 23:6135. https://doi.org/10.3390/ijms23116135